Band gaps and localization of surface water waves over large-scale sand waves with random fluctuations

Yu Zhang, Yan Li, Hao Shao, Yaozhao Zhong, Sai Zhang, and Zongxi Zhao

Phys. Rev. E **85**, 066319 — Published 25 June 2012

DOI: 10.1103/PhysRevE.85.066319

Band gaps and localization of surface water waves over large-scale sand waves with random fluctuations

Yu Zhang,[1,2,3,*] Yan Li,[2,3,*], Hao Shao,[2,3] Yaozhao Zhong,[2,3], Sai Zhang[1,3], and Zongxi Zhao[1,3]

[1] Key Laboratory of Underwater Acoustic Communication and Marine Information Technology of the Ministry of Education, Xiamen University, Xiamen, China

[2] State Key Laboratory of Marine Environmental Science, Xiamen University, Xiamen, China.

[3] College of Oceanography and Environmental Science, Xiamen University, Xiamen, China.

Correspondence and requests for materials should be addressed to Y. Z. or Y. L.

Abstract

Band structure and wave localization are investigated for sea surface water waves over large-scale sand wave topography. Sand wave height, sand wave width, water depth, and water width between adjacent sand waves have important impacts on band gaps. Random fluctuations of sand wave height, sand wave width, and water depth induce water wave localization. However, random water width produces a perfect transmission tunnel of water waves at a certain frequency so that localization would not occur no matter how large the disorder level is applied. Together with theoretical results, the field experimental observations in the Taiwan Bank suggest band gap and wave localization as the physical mechanism of sea surface water wave propagating over natural large-scale sand waves.

PACS number(s): 47.35.Bb, 04.30.Nk, 91.50.Ga

With the rapid development of photonic crystals and phononic crystals, the application of the Bloch theorem to water waves over periodically structured bottoms has recently received considerable attention [1-5]. It has been established both theoretically and experimentally that the interactions of water waves with structured bottoms can produce many interesting phenomena such as Bragg resonance and Anderson localization. For water waves propagating in periodic media, Bragg resonance induces complex band structures and the propagation of a water wave is forbidden within the band gap. In random media however, multiple scattering may lead to wave localization, a concept originally proposed by Anderson, [6] that explains electronic localization induced by disorders in electronic systems. By extending the ideas of band structures and localization to photonic crystals, phononic crystals, and water waves over periodic bottoms, a bridge has been formed between the disciplines of solid-state physics, optics, acoustics and fluid mechanics [6-11].

Although band structure and localization of surface water waves have recently been found in artificial and small-scale laboratory settings [1-5], the corresponding application in ocean waves over natural large-scale (hundreds of meters) sand waves has not yet been investigated. Tens to hundreds of sand waves naturally form a prominent periodic and rhythmic pattern in the offshore sandy seabed of shallow seas. In comparison with artificial structures, sand waves have special topographic features [12-18]. Water width between adjacent sand waves with significant random fluctuation is much larger than sand wave width, and sand wave height is comparable

with water depth. In ocean engineering, sand waves may interfere with anthropogenic activities, such as shipping lanes, pipelines on the seabed, and wind farms, thus significantly increasing the interest in water dynamics over sand waves. Satellite-borne synthetic aperture radar (SAR) imaging has been applied to reveal random topographic features of sand waves, such as height, length, and position [12]. Shao *et al.* [18] have applied satellite sensing sun glitter imaging of sand waves on the Taiwan Bank. The hydrodynamic interaction models have been previously applied to investigate the interaction of surface water wave with current over sand waves [12,17-19], however, none of these models has revealed the properties of band gaps and localization of surface water waves. Important impacts of sand wave random fluctuations on the band gaps of sea surface water waves has not yet been revealed.

In this paper, we investigate the band structure and wave localization of shallow sea surface water waves above natural large-scale uneven sand waves. The effects of sand wave random fluctuations on wave propagations are examined. Increasing the disorder level of random water width would not induce water wave localization at a certain frequency. The theoretical analyses, together with experimental observations in the Taiwan Bank, suggest band gap and wave localization of water wave over natural large-scale sand wave topography.

We consider the one-dimensional theoretical system to test the physical mechanism of band structure and wave localization of surface water waves over uneven sand wave bottoms. Detailed geophysical application requires determining the sand wave parameters based on the geophysically topographic features, which is

out of scope of this study and has been reported elsewhere [12-19]. The system shown in Fig. 1(a) describes N identical steps with width a and height H_a representing the periodically situated sand waves on the sea bottom. The water depth and width between adjacent sand waves are H_0 and b, and the water depth over the sand waves is $H_0 - H_a$. The water width b between adjacent sand waves is sufficiently larger than the sand wave width a. Based on previous studies [12,18], the typical parameter values of the large-scale sand wave system are used as: $\overline{a}$ = 60 m, $\overline{b}$ = 600 m, $\overline{H}_a$ = 20 m, and $\overline{H}_0$ = 30 m. Randomness of these parameters and the corresponding disorder levels are classified as:

(1) Sand wave width randomness. a is uniformly distributed with $[\overline{a}(1-\Delta a), \overline{a}(1+\Delta a)]$ and $a \geq 0$ leads to the disorder level $-1 \leq \Delta a \leq 1$.

(2) Sand wave height randomness. H_a is distributed with $[\overline{H}_a(1-\Delta H_a), \overline{H}_a(1+\Delta H_a)]$ and $H_a \leq \overline{H}_0$ leads to $1-\frac{\overline{H}_0}{\overline{H}_a} \leq \Delta H_a \leq \frac{\overline{H}_0}{\overline{H}_a}-1$.

(3) Water width randomness. b is within the range of $[\overline{b}(1-\Delta b), \overline{b}(1+\Delta b)]$ and $b \geq 0$ leads to the disorder level of $-1 \leq \Delta b \leq 1$.

(4) Water depth randomness. H_0 varies randomly between $[\overline{H}_0(1-\Delta H_0), \overline{H}_0(1+\Delta H_0)]$ and $H_0 \geq \overline{H}_a$ causes $\frac{\overline{H}_a}{\overline{H}_0}-1 \leq \Delta H_0 \leq 1-\frac{\overline{H}_a}{\overline{H}_0}$.

The equation governing the water wave over topographical bottom is described as [2,11]

$$\nabla\left(\frac{1}{k^2}\nabla\eta\right)+\eta=0 \tag{1}$$

where the wave number k satisfies $\omega^2 = gk\tanh(kH)$, η is the surface

displacement, and g is the gravity acceleration constant. Using the linear Eulerian equation of motion, the surface velocity vector $\vec{v}$ can be determined as $\frac{\partial \vec{v}}{\partial t} + g\nabla\eta = 0$ [2]. For a given frequency ω, k_0 in the water and k_a over the sand wave steps can be determined by using H_0 and $H_0 - H_a$. At the boundaries of the sand wave steps in Fig. 1(a), we have the following boundary conditions: both η and $\frac{\tanh(kH)}{k}\vec{n}\cdot\nabla\eta$ are continuous, where $\vec{n}$ denotes the outward normal vector at the boundaries. For one-dimensional surface water wave propagation, the water waves on the left and right ends can be solved from Eq. (1) as

$$\eta_L = A_L e^{ikx} + B_L e^{-ikx},$$

$$\eta_R = A_R e^{ikx} + B_R e^{ikx}, \tag{2}$$

where η_L and η_R are the surface displacements on the left and right ends of the sand wave system, A_L and B_L are the amplitudes of the incident and reflected waves. For the unit plane wave incidence, A_L = 1. A_R is the amplitude of the outgoing wave. The radiation boundary condition at the right end yields $B_R = 0$. Using the transfer matrix method [2,11], we can derive the transfer matrix T_i for the *i*th sandwave and the coefficients A_R and B_L, and thus obtain the transmission coefficient as $T = \prod_{i=1}^{N} T_i = |A_R|^2$. From the Bloch theorem, the eigenmodes of wave field in an infinite periodic medium can be written as $\eta(x) = u_K(x)e^{iKx}$, where $u_K(x)$ is the periodic function satisfying $u_K(x) = u_K(x + a + b)$ and K is the usual Bloch wave number. Thus, the dispersion relation is derived as

$$\cos[K(a+b)] = \cos(k_0 b)\cos(k_a a) - \frac{k_0^2 + k_a^2}{2k_0 k_a}\sin(k_0 b)\sin(k_a a) \tag{3}$$

Based on Eqs. (1)-(3), the frequency band structure of water waves over the periodic sand wave system can be obtained. Fig. 1(b) and (c) show the dispersion relation and the transmission coefficient T of the periodic sand wave structure respectively. The band gaps correspond to the significant transmission dips. For the frequency ranges outside of the grey region in Fig.1(b), the complex solution of K determines the forbidden energy bands or band gaps. Wave propagations are evanescent due to Bragg resonance and hence there are no transmission waves for the periodic sand wave structure. However, for the frequencies within the grey region, K has the real solution and water waves propagate through the sand wave system, corresponding to allowed energy bands or pass bands. Pass bands are separated by band gaps. Therefore, multiple scattering in the periodic sand wave system leads to complicated frequency band structures of water waves.

Topographic features of sand waves affect the band structure of water waves. To show this, Fig. 2(a)-(d) presents the dependencies of the band structure on sand wave height $H_a / \overline{H}_a$, sand wave width $a / \overline{a}$, water depth $H_0 / \overline{H}_0$, and water width $b / \overline{b}$. Here, the band structure shows a complicated relationship with frequency, differing from the single relationship in [11]. It may be associated with the much larger ratio a/b in Ref. [11] than the value in our sand wave system was used. As shown in Fig. 2(a), for sufficiently small H_a, band gaps disappear. With further increase in H_a, the band gaps show a complicated pattern: the lowest band gap becomes larger first but smaller later. Furthermore, when sand waves are as high as water depth, band gaps become so wide that water wave propagations are forbidden.

Fig. 2(b) shows that the band gap approaches a lower frequency in an oscillatory manner, with an increase of the sand wave width *a*. The water depth H_0 in Fig. 2(c) appears to have an inverse effect on band gaps as compared with H_a. $H_0 \to H_a$ gives the full band gap, and then the propagation of the wave is forbidden within the whole frequency range. In Fig. 2(d), with the increase of the water depth *b*, the band gaps approach lower frequencies more significantly than those in Fig. 2(b).

Furthermore, random structures of sand wave would complicate the transmission characteristics of the water wave. For random H_a, a, H_0, and b, Figs. 3(a) and (b) show the average transmission coefficient $\langle T \rangle$ at the right end of the sand wave system versus frequency *f*, where the disorder levels $\Delta H_a = \Delta a = \Delta H_0 = \Delta b = 0.3$, and the average results over 10000 random parameter generations for the whole sand wave array system were taken for each of these parameters. Random sand wave width *a* and height H_a could reduce wave transmissions, while random water width *b* and depth H_0 tend to smear out band structure. This is due to the fact that the change of H_a only affects k_a, however, the change of H_0 affects both k_0 and k_a, and thus produces a more significant effect on the band gaps. In addition, when the disorder levels of H_a, *a*, and H_0 are increased above some critical values, Anderson localizations appear.

However, for random water width *b*, Fig. 3(b) reveals an interesting delocalization phenomenon: wave localization is interrupted by a pass band around *f* = 0.08 Hz. At this resonant frequency, the sand wave width $\bar{a}$ equals to the

half-wavelength of the water wave. $|T_i|$ =1 at each sand wave unit causes the transmission coefficient $|T| = \left| \prod_{i=1}^{N} T_i \right|$ =1, and thus the water wave that can pass any single sand wave will then extend the entire sand wave system as well without transmission loss no matter how the water width *b* changes (that is how each of sand wave is situated). The sand wave system behaves like a single sand wave. We thus call this wave as perfect wave and the sand wave system as Perfect Transmission Tunnel (PTT) of water waves. When *f* slightly deviates from this value, transmission coefficient significantly decreases due to multiple scattering, particularly for large sand wave number *N*. PPT waves with $|T|$ =1 can also be found when the sand wave width $\bar{a}$ is an integer multiple of the half-wavelength of the water wave, e.g., $\bar{a} = m\lambda/2, (m = 1,2,\cdots)$. The numerical calculation based on the transfer matrix method [2,11] shows the consistency with this theoretical relationship in determining the resonant wavelength, as shown in Fig. 3(b). In order to further examine the effect of the disorder level Δb on wave localization, Fig. 3(c) shows the transmission $\langle T \rangle$ versus Δb, where insets are the energy distributions for Δb = 0.3 at three frequencies, 0.04 Hz, 0.08 Hz, and 0.12 Hz. For *f* = 0.04 Hz and 0.12 Hz, localization appears and $\langle T \rangle$ significantly decreases when Δb is increased above some critical value. Anderson localization greatly suppresses the water wave propagation. However, for *f* = 0.08 Hz, no matter how large Δb is, $\langle T \rangle$ remains almost unchanged and Anderson localization does not appear. PPT is produced in the sand wave system, and thus the PPT wave is extended to the whole system. Having an analogy with the resonant transmission of acoustic waves in random-dimer

medium [20], this transmission tunnel feature has not previously been reported in water wave systems. The finding presented in this study supports that increasing disorder level of a single random parameter may not always induce Anderson localization [21,22], even for one-dimensional water wave system.

Our theoretical investigations represent valuable exploration and provide important information to understand the field experiment observations in the Taiwan Bank. Detailed descriptions about the field experiment refer to the study by Shao et al [18]. High-resolution optical imaging was used to map submarine topography. Fig.4(a) shows the sea bottom topography of the Taiwan Bank and the sand wave stripes in a Landsat-5 Thematic Mapper satellite image, where the image was taken at 10:50 BJT in August 1998 under the spatial resolution of 30 m. Fig. 4(b) displays the enlarged area in Fig. 4(a) at 10:50 BJT on 11 August 1998, 10:21 BJT on 27 June 2005, and 10:27 BJT on 3 July 2007, respectively. Visible sand waves on the Taiwan Bank are stably situated and form a prominent periodic pattern of approximately parallel ridges. Between sand waves, the topography of the seabed is relatively flat. These topographic features of sand waves support the one-dimensional assumption of the above theoretical system. In Fig. 4(b), the depth-averaged horizontal velocity was measured by a 300 kHz vessel-mounted Acoustic Doppler Current Profilers (ADCP) at the time interval of 1.41 s, as shown in Fig. 4(c). Measurements were repeated 28 times along six sand waves. The limitation of the frequency resolution of ADCP causes that the reliably measured highest signal frequency should be much less than 0.35 Hz in order to avoid frequency aliasing. In addition, finite sand wave

number (such as six sand waves in Fig. 4(b)) causes the low frequency transmission property cannot be experimentally measured. Considering these two factors, we applied the eighth-order Butterworth band-pass filter to the theoretical model outputs in order to match the measured experimental results within the frequency range 0.04 Hz < f < 0.25 Hz.

The photograph in Fig. 4(d) displays the sea surface state when the vessel was heading across a sand wave crest where "R" and "S" represent rough and smooth surface states, respectively. The smooth and rough zones appear upstream and downstream of the sand wave crest, indicating their different spatiotemporal complexity [23,24]. As shown in Fig. 4(c), narrowband frequency currents were found above the sand wave crests, while broadband currents were observed in the troughs. The perfect waves with the m-order wavelength $2\overline{a}/m, (m = 1,2,\cdots)$ are dominantly observed within the smooth zones, while broadband waves are found within the rough zones. Fig. 5 compares the transmission coefficients derived from the experimental ADCP data and theoretical model output, where the sand wave system parameters are used as: $\overline{a}$ = 40 m, $\overline{b}$ = 600 m, $\overline{H}_a$ = 20 m, $\overline{H}_0$ = 25 m , and the disorder level Δb = 0.3, based on the field study by Shao et al [18], and the sand wave numbers N = 6 and 100 are used in the model, respectively. Clearly, the theoretical simulations show the qualitative consistency with the experimental measurements. Both theoretical and experimental results derived from six sand waves reveal that the non-perfect waves within the frequency range 0.1 < f < 0.15 Hz can be suppressed when propagating through the smooth zones, suggesting wave localization.

In particular, in the sand wave system with $N = 100$, the theoretical simulation reveals that the localization effect is more significant than that in $N = 6$, suggesting that including more sand waves can further suppress or filter out the non-perfect wave transmissions, although this study did not provide the experimental evidence to show this. Furthermore, the PPT waves with the wavelengths of $\bar{a}$ and $2\bar{a}$ in Fig. 5 can readily propagate through the sand wave systems with low energy decays. In experiments, the measured amplitude of higher-order PPT wave was lower than that of the lower-order waves. This is associated with the losses in the medium, which was treated as lossless in the theoretical models. These patterns of water waves from photography and ADCP correspond to the sand wave stripes in the Landsat-5 Thematic Mapper satellite image. Observations at these different spatial scales show the existences of band gaps and PPT for water waves in the Taiwan Bank.

In conclusion, we have investigated band structure and localization as the physical mechanism of sea surface water waves propagating through natural large-scale sand waves. The effects of sand wave height, sand wave width, water depth, and water width on the band gaps are analyzed. Furthermore, we investigate the wave localizations under the random fluctuations of these parameters. With the increase of disorder levels above some critical values, sand wave height, sand wave width, and water depth can induce Anderson localization of water waves. However, random water width produces the delocalized PTT of water waves at a certain frequency, and then continuously increasing its disorder level could not induce localization. PTT can significantly suppress other frequency components, and can be

a good candidate as frequency-control devices, such as filters. This might have potential application in ocean engineering, such as reducing the impact on sand waves dominating seabed from water waves. Finally, the field experiments in the Taiwan Bank were performed. The results from Landsat-5 Thematic Mapper satellite imaging, photography, and ADCP measurement shows band gap and wave localization outside laboratory conditions. Similar patterns can also be found in the North Sea, the Bisanseto Sea, and Georges Bank, suggesting that band gap and localization may represent common physical properties of ocean surface water waves above natural large-scale sand wave topography across the world.

This work was financially supported in part by the National Science Foundation of China (Grant Nos. 40876031 and 11174240) and the Natural Science Foundation of Fujian Province of China（No. 2012J06010）. We thank Professor X. H. Yan from for helpful discussions. We are grateful to Dr. Z. Y. Liu, Y. W. Jiang, Y. N. Chen, L. G. Tang for their suggestions in the early stage of this work and Sam Marshall for his help in editing the paper.

References

[1] M. Torres, J. P. Adrados, J. L. Aragon, P. Cobo, and S. Tehuacanero, and F. R. Montero de Espinosa, Phys. Rev. Lett. 90, 114501 (2003).

[2] M. J. Huang, C. H. Kuo, Z. Ye, Phys. Rev. E 71, 011201 (2005).

[3] X. Hu and C. T. Chan, Phys. Rev. Lett. 95, 154501 (2005).

[4] Y. Hu, G. Q. Miao, and R. J. Wei, Chin.Phys. Lett 26, 114303 (2009).

[5] T. S. Jeong, J. Kim, and H. Y. Park, Appl. Phys. Lett. 85, 1645 (2004)

[6] P. W. Anderson, Phys. Rev. 109, 1492 (1958).

[7] E. Yablonovitch, Phys. Rev. Lett. 58, 2059 (1987); S. John, Phys. Rev. Lett. 58, 2486 (1987); J.D. Joannopoulos, R.D. Meade, J.N. Winn, Photonic Crystals, Princeton Univ. Press, Princeton, NJ, 1995.

[8] Z. Liu, X. Zhang, Y. Mao, Y. Zhu, Z. Yang, C.T. Chan, P. Sheng, Science, 289, 1734 (2000).

[9] B. Liang, B. Yuan, and J. C. Cheng, Phys. Rev. Lett. 103, 104301 (2009).

[10] Z. Ye, Phys. Rev. E 67, 036623 (2003).

[11] Z. An and Z. Ye, Appl. Phys. Lett. 84, 15 (2004).

[12] Q. Zheng, L. Li, X. Guo, Y. Ge, D. Zhu, and C. Li, J. Geophys. Res., 111, C09028 (2006),.

[13] H. H. Van der Veen, S. Hulscher, M. Knaapen, Ocean Dynamics 56, 228–234 (2006).

[14] M. Knaapen and S. Hulscher, Regeneration of sand waves after dredging. Coastal Engineering 46(4), 277–289 (2002).

[15] G. F. Jordan, Science, 136, 839-848 (1962)

[16] C.-C. Mei, The Applied Dynamics of Ocean Surface Waves, World Scientific, Singapore, 1989.

[17] W. Alpers, J. Geophys. Res., 89, 10526-10546 (1984)

[18] H. Shao, Y. Li, and L. Li, J. Geophys. Res., 116, C06024 (2011).

[19] I. Hennings and D. Herbers J. Geophys. Res. 111, C10008(2006).

[20] A. Esmailpour1, M. Esmailpour, A. Sheikhan, M. Elahi, M. Reza Rahimi Tabar, and M. Sahimi, Phys. Rev. B, 78, 134206 (2008).

[21] D. M. Jovic, Y. S. Kivshar, C. Denz, and M. R. Belic, Phys. Rev. A 83, 033813 (2011)

[22] L.I. Deych, D. Zaslavsky, A.A. Lisyansky, Phys. Rev. Lett. 81, 5390 (1998).

[23] Y. Zhang and J. J. Jiang, Phys. Rev. E, 72, 035201 (2005).

[24] Y. Zhang, J. J Jiang, C. Tao, and E. Bieging, Chaos 17, 043114, (2007).

Figure Captions

(Color online) Fig.1 (a) One-dimensional sand wave system; (b) Dispersion relation; (c) Transmission coefficient T versus frequency f.

(Color online) Fig.2 Dependences of the band structure on (a) $H_a / \overline{H}_a$, (b) $a / \overline{a}$, (c) $H_0 / \overline{H}_0$, and (d) $b / \overline{b}$, where the band gaps are marked as red regions.

(Color online) Fig.3 (a) Average transmission coefficients $\langle T \rangle$ versus frequency f for the random fluctuations ΔH_a, Δa, and ΔH_0; (b) $\langle T \rangle$ versus f for $\Delta b = 0.3$ at N = 5, 100, and 1000 and $\Delta b = 0.3$ at N = 1000; (c) $\langle T \rangle$ versus Δb at 0.04 Hz, 0.08 Hz, and 0.12 Hz. Inset: energy distributions at these three frequencies for Δb = 0.3 indicated by the dashed line.

(Color online) Fig. 4 (a) Sand wave stripes in a Landsat-5 Thematic Mapper satellite image, where the image was taken at 10:50 BJT on 11 August 1998; (b) An enlarged area of sand waves at 10:50 BJT on 11 August 1998, 10:21 BJT on 27 June 2005, and 10:27 BJT on 3 July 2007; (c) Depth-averaged horizontal velocity measured by ADCP; (d) Photograph of the sea surface state above the sand waves, where "R" and "S" represent rough and smooth surface states, respectively.

Fig.5 Transmission coefficient $\langle T \rangle$ versus frequency f for the experimental data and theoretical model outputs with $N = 6$ and 100.

Figures

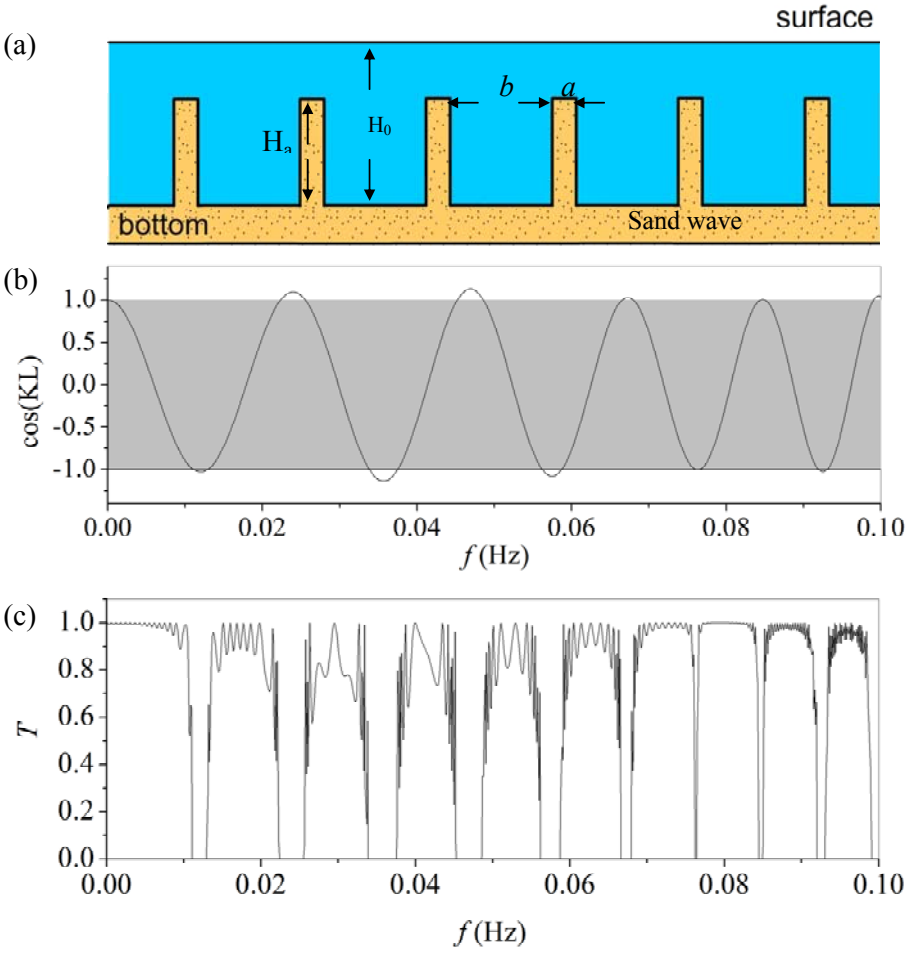

Figure 1

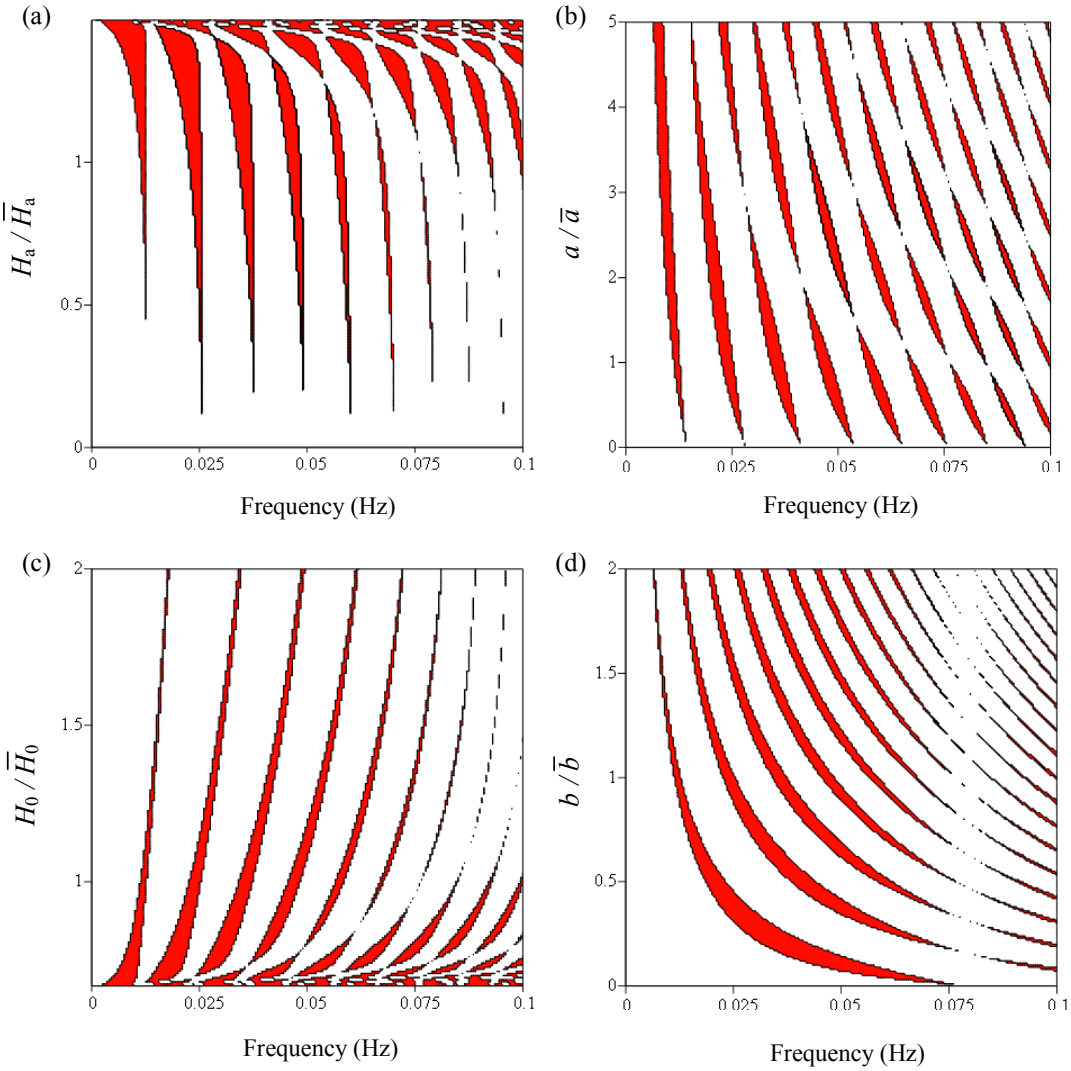
(a)
$H_a / \overline{H}_a$
Frequency (Hz)
(b)
$a / \overline{a}$
Frequency (Hz)
(c)
$H_0 / \overline{H}_0$
Frequency (Hz)
(d)
$b / \overline{b}$
Frequency (Hz)

Figure 2

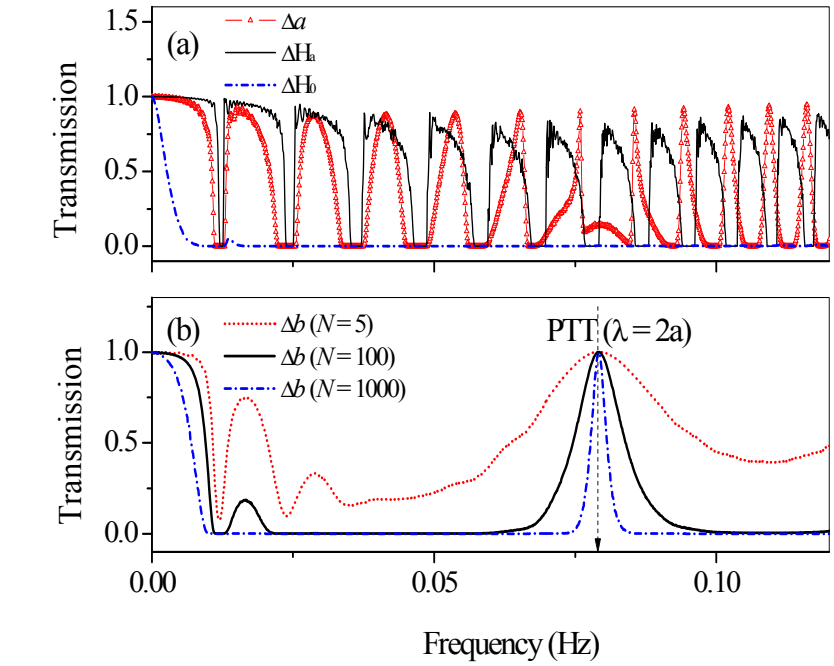
(a)
Δa
ΔH_a
ΔH_0
Transmission
(b)
Δb (N=5)
Δb (N=100)
Δb (N=1000)
PTT (λ=2a)
Transmission
Frequency (Hz)

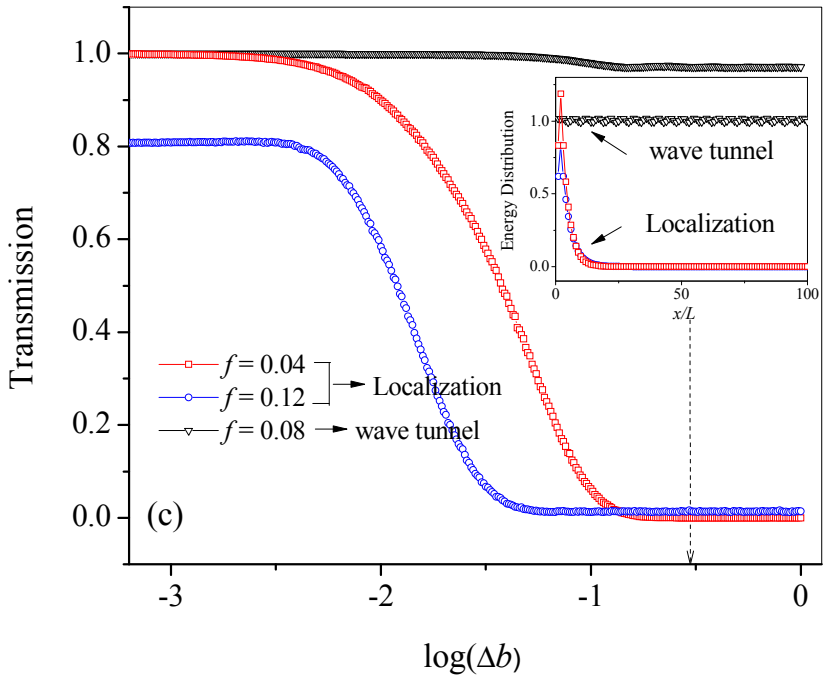
Transmission
(c)
f = 0.04
f = 0.12
Localization
f = 0.08
wave tunnel
Energy Distribution
wave tunnel
Localization
x/L
log(Δb)

Figure 3

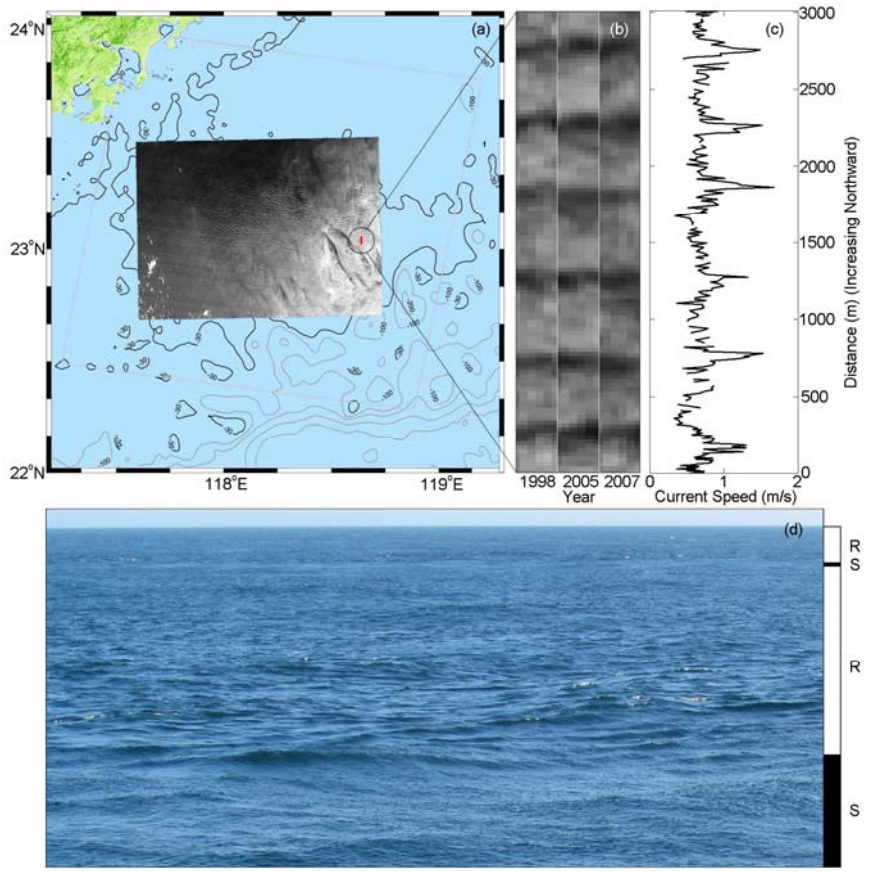

Figure 4

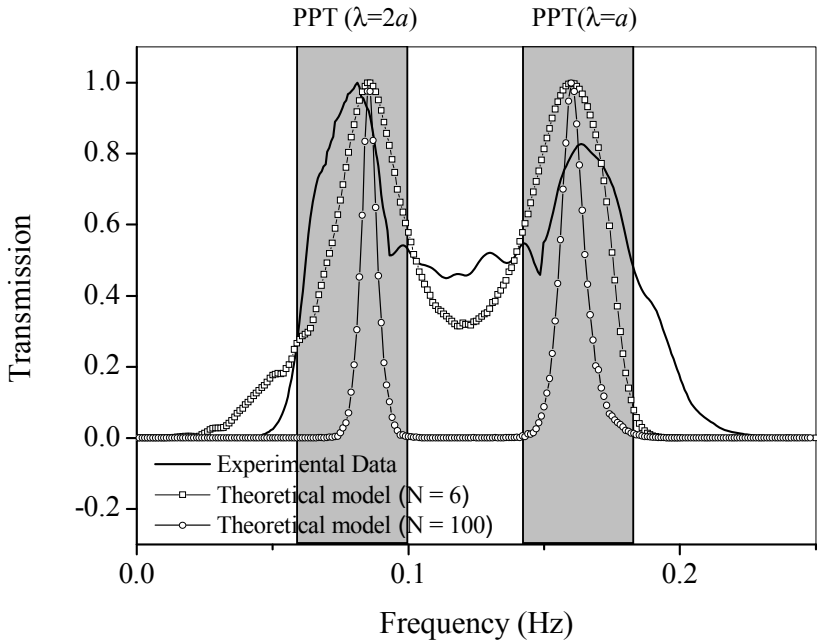

Figure 5